

The *Swift*/BAT High Latitude Survey: First Results

C. B. Markwardt,^{1,2} J. Tueller,² G. K. Skinner,³ N. Gehrels,² S. D. Barthelmy,² R. F. Mushotzky⁴

ABSTRACT

We present preliminary results from the first 3 months of the *Swift* Burst Alert Telescope (BAT) high galactic latitude survey in the 14–195 keV band. The survey reaches a flux of $\sim 10^{-11}$ erg cm⁻² s⁻¹ and has $\sim 2.7'$ (90% confidence) positional uncertainties for the faintest sources. This represents the most sensitive survey to date in this energy band. These data confirm the conjectures that a high energy selected AGN sample would have very different properties from those selected in other bands and represent a ‘true’ sample of the AGN population. We have identified 86% of the 66 high-latitude sources. 12 are galactic type sources and 44 can be identified with previously known AGN. All but 5 of the AGN have archival X-ray spectra, enabling the estimation of line of sight column densities and other spectral properties. Both of the $z > 0.11$ objects are Blazars. The median redshift of the others (excluding radio-loud objects) is 0.012. We find that the column density distribution of these AGN is bimodal with 64% of the non-blazar sources having column densities $N_H \geq 10^{22}$ cm⁻². None of the sources with $\log L_X > 43.5$ (c.g.s. units) show high column densities and very few of the lower L_X sources have low column densities. Based on these data, we expect the final BAT catalog to have >200 AGN and reach fluxes of less than $\sim 10^{-11}$ erg cm⁻² s⁻¹ over the entire sky.

Subject headings: surveys, galaxies: active, gamma rays: observations

¹Department of Astronomy, University of Maryland, College Park, MD 20742; craigm@milkyway.gsfc.nasa.gov

²Astroparticle Physics Laboratory, Mail Code 661, NASA Goddard Space Flight Center, Greenbelt, MD 20771

³Centre d’Etude Spatiale des Rayonnements, CNRS/UPS, 9 Avenue du Colonel Roche, 31028 Toulouse Cedex 04, France

⁴X-ray Astrophysics Laboratory, Mail Code 662, NASA Goddard Space Flight Center, Greenbelt, MD 20771

1. Introduction

It is now realized that most AGN have high column densities of absorbing material in our line of sight which significantly change their observable properties across much of the electromagnetic spectrum. This material can effectively hide the soft X-ray, optical and UV signatures of an active nucleus. There are two spectral bands, the hard X-ray ($E > 20$ keV) and the mid-IR (5–50 μm), where this obscuring material is relatively optically thin for column densities less than 10^{24} cm^{-2} . Thus these bands are optimal for unbiased AGN searches (Treister & Urry 2005). Recent observations with the Spitzer observatory are revealing many AGN via their IR emission (Stern et al. 2005), but this process is hampered by strong emission from star formation and the lack of a unique spectral signature to separate AGN from normal galaxies.

There has been little progress in hard X-ray surveys in the last 25 years due to a lack of instruments with sufficient angular resolution to identify counterparts in other wavelength bands and with sufficient sky coverage and sensitivity to produce a large sample. INTEGRAL observations are predominantly in the galactic plane and high latitude coverage is patchy.

We report here preliminary results from the *Swift* BAT high galactic latitude ($|b| > 19^\circ$) survey. Although this report is based on only the first 3 months, we detect 66 sources above 5.5σ significance. Only 9 of the sources do not have firm identifications. Being basically unaffected by obscuration, BAT determines the intrinsic 14–195 keV luminosity, L_X . The survey is already about ten times more sensitive than the previous large solid angle survey in this band from HEAO-1 A4 (Levine et al. 1984) and covers the whole sky at $\sim 1 - 3 \times 10^{-11}$ $\text{erg cm}^{-2} \text{s}^{-1}$.

2. Observations

The BAT instrument on *Swift* is a very large field of view coded aperture hard X-ray telescope with a CdZnTe detector array ($\sim 1/8$ of the sky is at least partially coded at any one time). While primarily designed for the detection and rapid dissemination of gamma-ray burst positions, the BAT is also an effective all-sky hard X-ray monitor and survey instrument. The BAT focal plane consists of a 0.5 m^2 CdZnTe array, divided into 32768 detectors, providing good sensitivity and energy resolution in the 14–195 keV energy range. BAT can reach ~ 65 mCrab in a typical 450 s integration and typically covers 50–80% of the sky each day. The effective exposure during the first 3 months varies over the sky from 200 to 800 ks. Away from the galactic center region, the sensitivity scales as the square root of the exposure and so varies by a factor two (Figure 1). The statistical quality of the BAT

survey map can be assessed by comparing positive and negative fluctuations. Figure 2 shows the excess in positive fluctuations of individual pixels. With the reconstruction algorithm used, each source appears in several correlated pixels; the source detection significance is approximately the peak value. Since the noise distribution is symmetric, and there are no pixels $< -5.5\sigma$, we expect no false detections above our $+5.5\sigma$ threshold. We estimate that the sensitivity limit is <0.5 mCrab for $\sim 50\%$ of the sky.

The survey is based on individual sky images produced using FFTs to correlate the data from one pointing (typically a few 1000 s) with the mask pattern. The FFT is oversampled by a factor of 2 to prevent loss of sensitivity at bin boundaries. Each image is a tangent plane projection with a point spread function (PSF) of $22'$ full-width at half maximum at the image center. A single image has very non-uniform sensitivity due to partial coding at the edges (we exclude regions with $< 15\%$ partial coding). Background variations around the orbit and other systematic effects cause the noise to vary both spatially and temporally. To achieve a good sensitivity it is necessary to clean from the data the effects of bright sources and of constant background non-uniformities. The noise in the resulting cleaned images is often near the statistical limit. However, some excess noise remains, so uncertainties used in this analysis are calculated from the observed r.m.s. noise in the images. These images are interpolated and combined to form an all-sky map with $5'$ sampling. Pixel weights are based on the local r.m.s. noise in the component images. The r.m.s. error is then recalculated and the image is searched for local maxima greater than 5.5σ . Each maximum is least squares fitted with a gaussian PSF to derive a position and flux.

The output from two separate analysis pipelines (developed by authors C. M. and J. T. vs. G. S.), using somewhat different background correction and image combination algorithms, have been compared and they agree well.

Figure 2 shows the BAT confidence contours plotted on the images of two known sources, illustrating the variation in position accuracy with source significance. The systematic and statistical errors are estimated by comparing ~ 1800 BAT position measurements with the known positions for ~ 60 X-ray sources. The precision improves from $\sim 3.7'$ (95% confidence radius) for sources at $\sim 6\sigma$ significance to $\sim 0.9'$ at $> 20\sigma$ significance. For these early data, the flux calibration is uncertain by $\sim 30\%$ as a result of the spectrally dependent count rate to flux conversion. At present, the calculation of exposure as a function of sky position is still approximate. Consideration of the $\log N - \log S$ distribution and of source spectra are thus left to a later paper.

3. Results

Our list contains 66 sources at $|b| > 19^\circ$, of which 12 can be identified as galactic or SMC/LMC objects, and 45 have clear identifications with cataloged optical objects, (e.g. the catalog of Veron-Cetty & Veron (2003)). Except for the Coma cluster, all 45 are known AGN (Table 1). Of the 9 remaining detections, we have tentative identifications for four cataloged objects which do not have bright *ROSAT* counterparts. Two of the unidentified detections are *RXTE* slew survey sources (XSS J05054–2348 and XSS J12389–1614, which have nearby bright galaxies). Three sources do not have obvious optical counterparts. All but five of the cataloged AGN (ESO 297–018, NGC 1142, MCG +04–22–042, ESO 323–077 and Mrk 1498) have published or available X-ray spectra.

The identified sources are dominated by low luminosity, low redshift objects. There are three Blazars (3C 273, 4C +71.07, and Mrk 421) and five radio loud AGN (3C 390.3, Cen A, 3C 120, 4C +74.26 and Mkn 1498), consistent with the roughly 10% of all AGN that are thought to be radio loud. The line of sight column densities and X-ray fluxes of the 39 objects (3 Blazars and 36 Seyferts) with X-ray spectra have been obtained primarily by ASCA or *BeppoSAX* (e.g., Lutz et al. 2004). In those cases where Lutz et al. do not quote a column density, we have used results from the Tartarus ASCA data base or from archival *XMM-Newton* or *Chandra* data. Because the Tartarus data base uses only simple spectral models, the precision of column densities is only ± 0.5 dex. However this is sufficient to categorize the objects as heavily absorbed or not.

Assuming a typical power law spectrum ($\Gamma \sim 1.7$), a conservative absorption column ($\log N_H = 24$), and the BAT limiting flux, we derive a 2–10 keV limiting flux of $\sim 10^{-12}$ erg cm $^{-2}$ s $^{-1}$. Using the flux distribution of Moretti et al. (2003), we expect < 0.01 chance sources per BAT error circle, and hence < 1 misidentification overall.

Excluding the Blazars, the median redshift is $z \sim 0.012$ (the mean is 0.018), giving a median $\log L_X$ 43.3 in the 14–195 keV band and a median column density of $\log N_H = 22.6$. The X-ray luminosity against column density scatter plot for the non-blazars (Figure 3) shows an absence of high column density, highly luminous sources.

A surprising result from our survey is the very high fraction of identified sources. In HEAO-1 (Piccinotti et al. 1982), $\sim 1/2$ of the 2–10 keV X-ray selected AGN were ‘new’ objects. In the deep *Chandra* surveys (Barger et al. 2005), $\sim 1/3$ of all sources did not show a strong optical AGN signature. We thus anticipated that many of the BAT hard X-ray selected objects would not have a cataloged AGN counterpart. The high identification rate of this first BAT sample shows that, contrary to some suggestions, classical optical techniques have been successful at finding objects with high line of sight column densities in

the low redshift universe.

Defining an absorbed object as one with $\log N_H \geq 22.0$ (Ueda et al. 2003), the ratio of absorbed to unabsorbed objects is 1.8:1 (excluding the Blazars), somewhat less than suggested by the standard ‘unified’ AGN models. The distribution of column densities is approximately bimodal (Figure 3). The fact that a ratio of 1:3 was found by Sazonov & Revnivtsev (2005) for identified sources in the *RXTE* slew survey indicates the strength of the bias towards the detection of unobscured objects in 2–10 keV low redshift X-ray surveys.

The distribution of optical classes of the BAT sources is very different from those in an optical color selected or line selected survey, with only 20% of the objects being optically classified as Seyfert Is, compared with $\sim 40\%$ in optical surveys at low redshift. This illustrates the power of a hard X-ray survey to find all classes of AGN.

Given the limited sensitivity of the BAT survey (all but 15% of the sources are brighter than $\sim 3 \times 10^{-11}$ erg cm $^{-2}$ s $^{-1}$), it is surprising that many are not in the HEAO-1 A2 catalog (Piccinotti et al. 1982). Most of the 18 objects not seen by HEAO-1 were clearly missed due to obscuration, since 12 of them have column densities greater than 10^{23} cm 2 . Three of these ‘missing’ objects (Akn 120, 3C 390.3 and 4C +74.26) are known to be highly variable. Akn 120 is the only narrow line Seyfert I in the BAT sample, which is consistent with the known steep high energy spectrum of these objects (Brandt et al. 1997).

Comparison of the HEAO-1 2–10 keV fluxes with the more recent *RXTE* fluxes (Revnivtsev et al. 2004) shows a variation of $\sim 60\%$ in flux, with only $\sim 10\%$ of the objects showing more than a factor of two variability across the ~ 20 years between these two data sets. While the *RXTE* slew survey is much more sensitive than BAT for unabsorbed objects, at least 8 BAT sources were not detected in the *RXTE* data (Mrk 348, Mrk 1498, NGC 3081, UGC 5037, NGC 1142 and NGC 1365). Of these, 3 have high column densities, and 3 do not have X-ray spectra.

Most (36/44) of the AGN have cataloged *ROSAT* fluxes (taken from the ROSPSPC catalog when available, otherwise taken from the *ROSAT* all sky survey data base). There is little or no correlation between the BAT and *ROSAT* fluxes. This is not surprising because the scatter in the *ROSAT* rates is dominated by the effect of different degrees of intrinsic absorption in the sources, whereas these have relatively little effect in the BAT energy range. This illustrates the difficulty of constructing a complete AGN sample from soft X-ray data. Since there is a very strong relation between optical nuclear and soft X-ray flux (Mushotzky 2004; Barger et al. 2005), samples based on optical data are subject to similar difficulties.

A crucial component for models of the X-ray background is the distribution of N_H values. Our data determine this distribution, in an unbiased way, for the first time. There

is little evidence for variation of N_H with L_X below $\log L_X = 43.5$, but above this luminosity $\langle \log N_H \rangle$ drops to ~ 20.9 compared with 22.9 below it. This break point occurs around the characteristic luminosity of AGN in the *Chandra* surveys of $\log L_X \sim 43.8$ (corrected for the band pass differences; Barger et al. (2005)) and is probably related to this feature. The only object at $\log L_X > 43.5$ with a high line of sight column density is EXO 055620–3820.2. This object (Crenshaw & Kraemer 2001) has complex absorbing material (Quadrelli et al. 2003) that seems to be associated with the host galaxy. In the entire BAT AGN sample, including low latitude objects, there are no extra-galactic objects with $\log L_X < 42.5$ which are not heavily absorbed. This is not a selection effect. While such objects clearly exist (e.g., NGC 3998 Ptak et al. 2004), they must be rare. The BAT data establish the $z = 0$ relationship of absorption and luminosity needed to model the evolution of hard X-ray sources e.g. (Mateos et al. 2005).

Recently (Hopkins et al. 2005a,b) have constructed physical models which apparently can explain much of the observed evolution of AGN and the differences between samples in different wavelength bands. These models only correctly predict the observed absorption distribution when they include cold material in the line of sight. The predicted distribution of column densities and the predicted loose correlation between L_X and N_H are in rough agreement with the BAT data. However this model completely misses the observed sharp reduction in high N_H objects at high luminosity.

Comparing the BAT luminosities with 10 or 3.5 μm IR luminosities (e.g., Lutz et al. 2004; Gorjian et al. 2004) shows little or no correlation. A similar lack of correlation of the ratio of the IR to BAT flux ratios with X-ray absorption indicates a wide scatter between observed IR properties and the intrinsic properties of the AGN. Previous work (Krabbe 2001) had reported a strong correlation between the 10 μm IR fluxes and the hard X-ray fluxes, naïvely expected if the near IR is dominated by AGN light which is relatively unabsorbed. However in the new Spitzer results (Francheschini et al. 2005) such a correlation is only seen for type I objects. This lack of correlation may be due to additional IR radiation from star formation, high optical depths even at 10 μm , or additional scatter introduced by reprocessing of the nuclear radiation in the IR. The absence of a correlation makes the analysis using the unified models to connect the IR and X-ray data suspect (Treister & Urry 2005). Similarly there is little or no correlation between BAT and [OIII] luminosities.

The BAT sample allows a true measure of the nature of the low z hosts of active galaxies. Of the 24 objects in the sample with “T” types as categorized in the RC3 (de Vaucouleurs et al. 1991), 9 have “T” types < 0 , indicating a spheroidal host fraction of $\sim 40\%$, similar to that seen in the *Chandra* surveys and the SDSS data (Kauffmann & Heckman 2005; Grogin et al. 2005). This is much larger than the fraction in classical optical surveys. However,

none of the objects is classified as a giant elliptical galaxy, which is rather different than the *Chandra* surveys, probably due to the low redshifts probed by the BAT sample.

It is interesting to note that all the broad line radio galaxies detected by HEAO-1 (Marshall et al. 1978) (3C 111.0, 3C 120, 3C 382, 3C 390.3) are detected by the BAT, indicating that radio galaxies may have systematically harder X-ray spectra in the BAT band than Seyferts.

4. Conclusions

We have shown the usefulness of a sensitive, large solid angle hard X-ray survey in defining the nature of the AGN population. As predicted by models of the X-ray background, the dominant source population are absorbed AGN and are very different from an optically or soft X-ray derived AGN population. We derive the true distribution of absorbing column density with X-ray luminosity and find that while virtually all sources with $\log L_X < 43.5$ are absorbed, those with higher luminosities are mostly unabsorbed. This luminosity corresponds to the break in the X-ray luminosity function and is a strong clue to the nature of the absorbing material and the origin of the feature in the luminosity function. We find little correlation between other measures of the luminosity of absorbed AGN (e.g. [OIII], 3.5 or 10 μm luminosity) and the hard X-ray luminosity, suggesting that previous techniques may have previously unsuspected biases in finding and measuring absorbed AGN. The high identification fraction ($\sim 86\%$) is somewhat unexpected given our previous knowledge of these sources and bodes well for the much larger samples that the BAT will obtain over the next two years.

Further work on the present sample will include determination of the $\log N - \log S$ of the hard X-ray sample, the luminosity function, spectral and temporal analysis of the BAT selected AGN directed towards a detailed understanding of the relationship of the hard X-ray to other wavelength bands. Preliminary estimates indicate that an eventual 3(+) year BAT high latitude catalog will have more than 200 AGN, which will allow extensive correlation analyses.

We thank the entire BAT and *Swift* teams for their extensive efforts which have made this work possible.

REFERENCES

- Barger, A. J., Cowie, L. L., Mushotzky, R. F., Yang, Y., Wang, W.-H., Steffen, A. T., & Capak, P. 2005, *AJ*, 578, 129
- Brandt, W. N., Mathur, S., & Elvis, M. 1997, *MNRAS*, 285, L25
- Crenshaw, D. M., & Kraemer, S. B. 2001, *ApJ* 562, L29
- Francheschini, A., et al. 2005, *AJ*, in press (astro-ph/0412476)
- Gilli, R., Maiolino, R., Marconi, A., Risaliti, G., Dadina, M., Weaver, K. A., & Colbert, E. J. M. 2000, *A&A*, 355, 485
- Gondoin, P., Orr, A., Lumb, D., & Siddiqui, H. 2003, *A&A*, 397, 883
- Gorjian, V., Werner, M. W., Jarrett, T. H., Cole, D. M., & Ressler, M. E. 2004, *ApJ*, 605, 156
- Grogin, N. A., et al. 2005, *ApJ*, 627, L97
- Hopkins, P. F., Hernquist, L., Cox, T. J., Di Matteo, T., Robertson, B., Springel, V. 2005a, *ApJ*, submitted (astro-ph/0506398)
- Hopkins, P. F., Hernquist, L., Cox, T. J., Robertson, B., Springel, V. 2005b, *ApJ*, submitted (astro-ph/0508167)
- Krabbe, A., Böker, T., Maiolino, R. 2001, *ApJ*, 557, 626
- Kauffmann, G. & Heckman, T. 2005, *Phil. Trans. Roy. Soc.* in press, (astro-ph/0406219)
- Komossa, S., Burwitz, V., Hasinger, G., Predehl, P., Kaastra, J. S., Ikebe, Y. 2003, *ApJ*, 582, L15
- Levine, A., et al. 1984, *ApJS*, 54, 581
- Lutz, D., Maiolino, R., Spoon, H. W. W., & Moorwood, A. F. M. 2004, *A&A*, 418, 465
- Marshall, F. E., Boldt, E. A., Holt, S. S., Mushotzky, R. F., Rothschild, R. E., Serlemitsos, P. J., Pravdo, S. H. 1979, *ApJS*, 40, 657
- Mateos, S., et al. 2005, *A&A*, 433, 855
- Moretti, A., Campana, S., Lazzati, D., & Tagliaferri, G. 2003, *ApJ*, 588, 696

- Mushotzky, R.F. 2004, in *Supermassive Black Holes in the Distant Universe*, ed. A. J. Barger (Dordrecht: Kluwer), 53
- Perlman, E. S., et al. 2005, *ApJ*, 625, 727
- Piccinotti, G., Mushotzky, R. F., Boldt, E. A., Holt, S. S., Marshall, F. E., Serlemitsos, P. J., Shafer, R. A. 1982, *ApJ*, 253, 485
- Ptak, A., Terashima, Y., Ho, L. C., & Quataert, E. 2004, *ApJ*, 606, 173
- Quadrelli, A., Malizia, A., Bassani, L., & Malaguti, G. 2003, *A&A*, 411, 77
- Revnivtsev, M., Sazonov, S., Jahoda, K., & Gilfanov, M. 2004, *A&A*, 418, 927
- Sazonov, S. Yu., & Revnivtsev, M. G. 2005, *A&A*, 423, 469
- Spergel, D. N., et al. 2003, *ApJS*, 148, 175
- Stern, D., et al. 2005, preprint (astro-ph/0410523)
- Treister, E., Urry, C. M. 2005, *ApJ*, accepted (astro-ph/0505300)
- Turner, T. J., Nandra, K., Turcan, D., & George, I. M. 2001, *AIP Conf. Proc.* 599: X-ray Astronomy: Stellar Endpoints, AGN, and the Diffuse X-ray Background, 599, 991
- Ueda, Y., Akiyama, M., Ohta, K., & Miyaji, T. 2003, *ApJ*, 598, 886
- de Vaucouleurs, G., de Vaucouleurs, A., Corwin, H. G., Buta, R. J., Paturel, G., & Fouque, P. 1991, Volume 1-3, XII, 2069 pp. 7 figs.. Springer-Verlag Berlin Heidelberg New York,
- Veron-Cetty, M.-P., & Veron, P. 2003, *A&A*, 412, 399, <http://vizier.u-strasbg.fr/viz-bin/VizieR>
- Vignali, C., & Comastri, A. 2002, *A&A*, 381, 834

Table 1. BAT Detections of AGN (On-line only table)

SWIFT Name	R.A. (J2000) °	Decl. (J2000) °	Err. ^a ′	Identification	Offset ′	z	$\log N_H$ cm^{-2}	Ref.	$\log L_X$ ^{b,c,d} $\text{erg s}^{-1} \text{cm}^{-2}$	RL ^e	Type ^f
J0048.8+3157	12.200	31.963	4.8	Mrk 348	0.4	0.0150	22.9	1	43.7	N	Sy
J0123.7–3502	20.942	-35.040	4.4	NGC 526A	2.3	0.0191	22.3	2	43.8	N	Sy
J0123.9–5848	20.978	-58.811	4.9	Fairall 9	1.2	0.0470	20.4	2	44.3	N	Sy
J0138.9–4005	24.730	-40.094	5.3	ESO 297–018	6.0	0.0252	43.4	N	Sy
J0238.2–5216	39.562	-52.275	5.2	ESO 198–024	5.0	0.0455	21.0	1	44.2	N	Sy
J0255.0–0009	43.765	-0.158	4.7	NGC 1142	2.6	0.0288	44.3	N	Sy
J0333.5–3608	53.377	-36.143	3.2	NGC 1365	1.2	0.0055	23.6	2	42.6	N	Sy
J0433.1+0521	68.288	5.362	3.7	3C 120	0.7	0.0330	21.2	1	44.4	Y	Sy
J0451.8–0347	72.964	-3.799	5.1	MCG –01–13–025	2.5	0.0159	20.5	3	43.3	N	Sy
J0516.3–0008	79.078	-0.137	4.6	Ark 120	2.0	0.0323	20.3	2	43.9	N	Sy
J0557.8–3822	89.466	-38.371	3.8	EXO 055620–3820.2	3.0	0.0339	22.2	1	44.2	N	Sy
J0615.9+7100	93.996	71.000	3.3	Mrk 3	2.9	0.0135	24.0	2	43.6	N	Sy
J0841.7+7052	130.437	70.875	4.5	4C +71.07	2.1	2.1720	21.0	1	48.3	Y	Bl
J0924.1+2256	141.038	22.945	4.7	MCG +04–22–042	6.4	0.0323	43.9	N	Sy
J0924.8+5216	141.220	52.280	4.2	Mrk 110	3.1	0.0353	20.6	1	43.9	N	Sy
J0945.6–1420	146.411	-14.343	4.1	NGC 2992	1.3	0.0077	22.0	4	42.9	N	Sy
J0959.4–2250	149.874	-22.848	4.4	NGC 3081	1.3	0.0080	23.5	5	43.0	N	Sy
J1023.5+1952	155.875	19.870	3.2	NGC 3227	0.3	0.0039	22.8	6	42.4	N	Sy
J1031.6–3450	157.924	-34.836	4.1	NGC 3281	2.4	0.0107	24.3	7	42.8	N	Sy
J1104.5+3813	166.129	38.218	3.2	Mrk 421	0.9	0.0300	20.3	8	44.1	Y	Bl
J1106.5+7235	166.631	72.599	2.9	NGC 3516	2.2	0.0088	21.2	1	43.2	N	Sy
J1138.9–3744	174.743	-37.740	2.5	NGC 3783	0.7	0.0097	22.5	2	43.3	N	Sy
J1209.6+4343	182.418	43.730	5.0	NGC 4138	3.3	0.0030	22.8	3	42.1	N	Sy
J1210.5+3924	182.627	39.412	1.1	NGC 4151	0.5	0.0033	22.5	2	43.0	N	Sy
J1225.8+1239	186.452	12.664	1.9	NGC 4388	0.4	0.0084	23.6	2	43.6	N	Sy
J1229.1+0203	187.283	2.052	2.3	3C 273	0.3	0.1583	20.5	1	46.1	Y	Bl
J1235.6–3953	188.909	-39.894	1.9	NGC 4507	0.9	0.0118	23.5	2	43.8	N	Sy
J1239.6–0518	189.900	-5.304	4.0	NGC 4593	2.6	0.0090	20.3	2	43.3	N	Sy
J1306.8–4023	196.706	-40.386	4.9	ESO 323–077	4.7	0.0150	43.4	N	Sy
J1322.5–1645	200.630	-16.759	5.0	MCG –03–34–064	2.5	0.0165	23.5	5	43.4	N	Sy
J1325.4–4300	201.362	-43.014	1.0	Cen A	0.4	0.0018	22.7	1	42.6	Y	Sy
J1349.3–3018	207.335	-30.310	2.0	IC 4329A	0.2	0.0161	21.6	1	44.1	N	Sy
J1353.1+6916	208.295	69.269	5.1	Mrk 279	2.5	0.0305	20.5	1	44.0	N	Sy
J1413.2–0312	213.316	-3.207	2.3	NGC 5506	0.3	0.0062	22.5	2	43.1	N	Sy
J1442.4–1713	220.602	-17.233	4.5	NGC 5728	1.2	0.0093	23.5	9	43.2	N	Sy
J1628.0+5144	247.017	51.747	4.5	Mrk 1498	1.7	0.0547	44.5	Y	Sy
J1838.2–6526	279.553	-65.438	3.8	ESO 103–035	1.0	0.0133	23.2	1	43.2	N	Sy
J1842.0+7945	280.514	79.754	3.1	3C 390.3	1.1	0.0561	21.0	1	44.8	Y	Sy
J2043.0+7504	310.763	75.073	4.7	4C +74.26	4.0	0.1040	21.6	3	45.3	Y	Sy
J2044.3–1045	311.076	-10.765	4.9	Mrk 509	3.3	0.0344	20.7	1	44.4	N	Sy
J2052.1–5703	313.037	-57.056	4.3	IC 5063	1.2	0.0113	23.3	1	43.4	N	Sy
J2201.8–3152	330.461	-31.882	3.7	NGC 7172	2.5	0.0087	22.9	1	43.4	N	Sy
J2254.0–1732	343.522	-17.541	4.8	MR 2251–178	2.5	0.0640	20.8	1	45.0	N	Sy
J2318.4–4223	349.609	-42.391	3.6	NGC 7582	1.3	0.0053	23.0	1	42.5	N	Sy

Note. — *a* Error radius (99% conf.); *b* BAT Luminosity, 14–195 keV; *c* Estimated systematic error: +20%, –50%; *d* Assumes a *WMAP* cosmology ($H_0 = 71 \text{ km s}^{-1} \text{ Mpc}^{-1}$, $\Omega_M = 0.27$, $\Omega_\Lambda = 0.73$; Spergel et al. 2003) *e* Radio Loud?; *f* Sy=Seyfert; Bl=Blazar

References. — (1) Turner et al. 2001; (2) Lutz et al. 2004; (3) This work (*XMM-Newton*); (4) Gilli et al. 2000; (5) This work (*ASCA*); (6) Gondoin et al. 2003; (7) Vignali & Comastri 2002; (8) Perlman et al. 2005; (9) This work (*Chandra*)

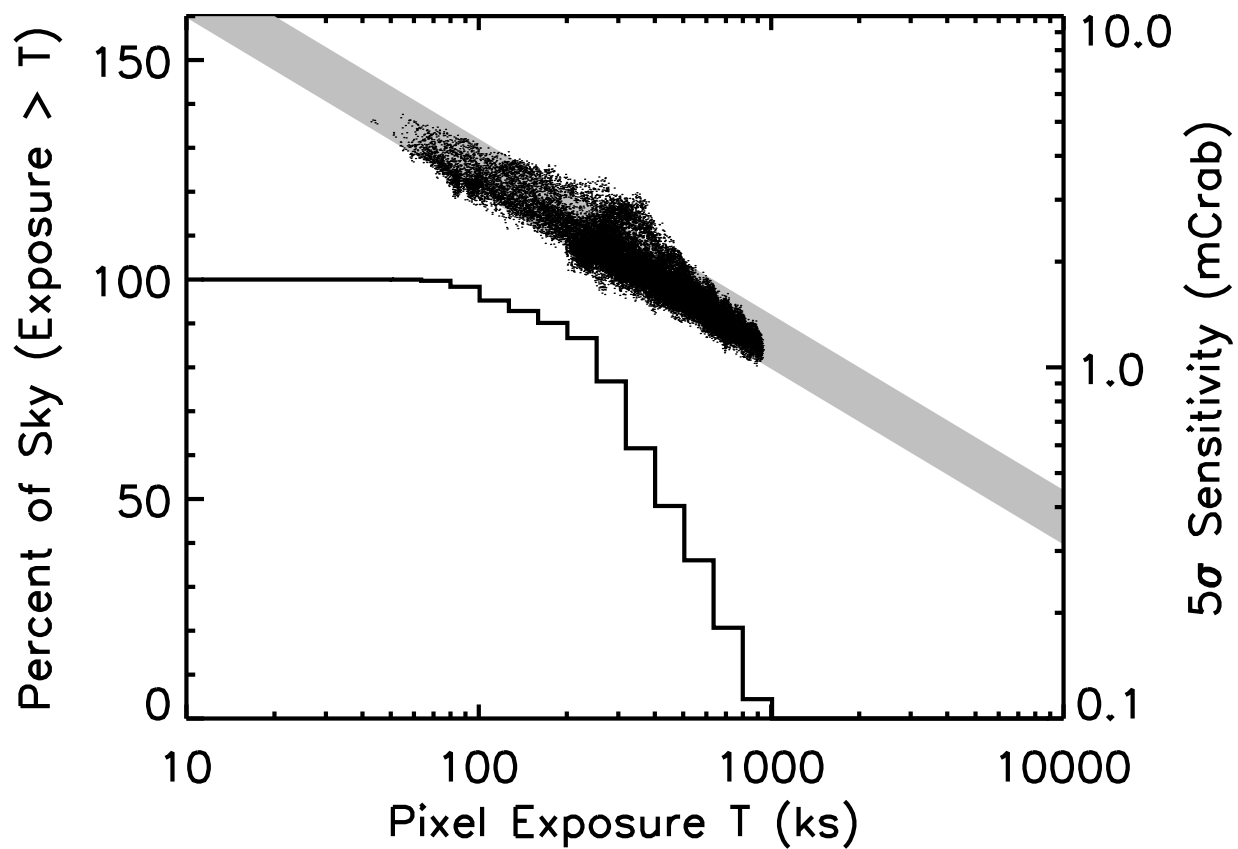


Fig. 1.— BAT all-sky sensitivity and exposure statistics. Dots (top; right scale) represent the 5σ pixel sensitivity threshold. The gray band corresponds to the function $(8.5 \pm 1.5)\text{mCrab}(T/20\text{ks})^{-0.5}$, extrapolated to larger exposures T . The solid line (bottom; left scale) is the cumulative sky coverage with an exposure of greater than T , expressed as a percentage of the solid angle analyzed ($100\% = 0.67 \times 4\pi$).

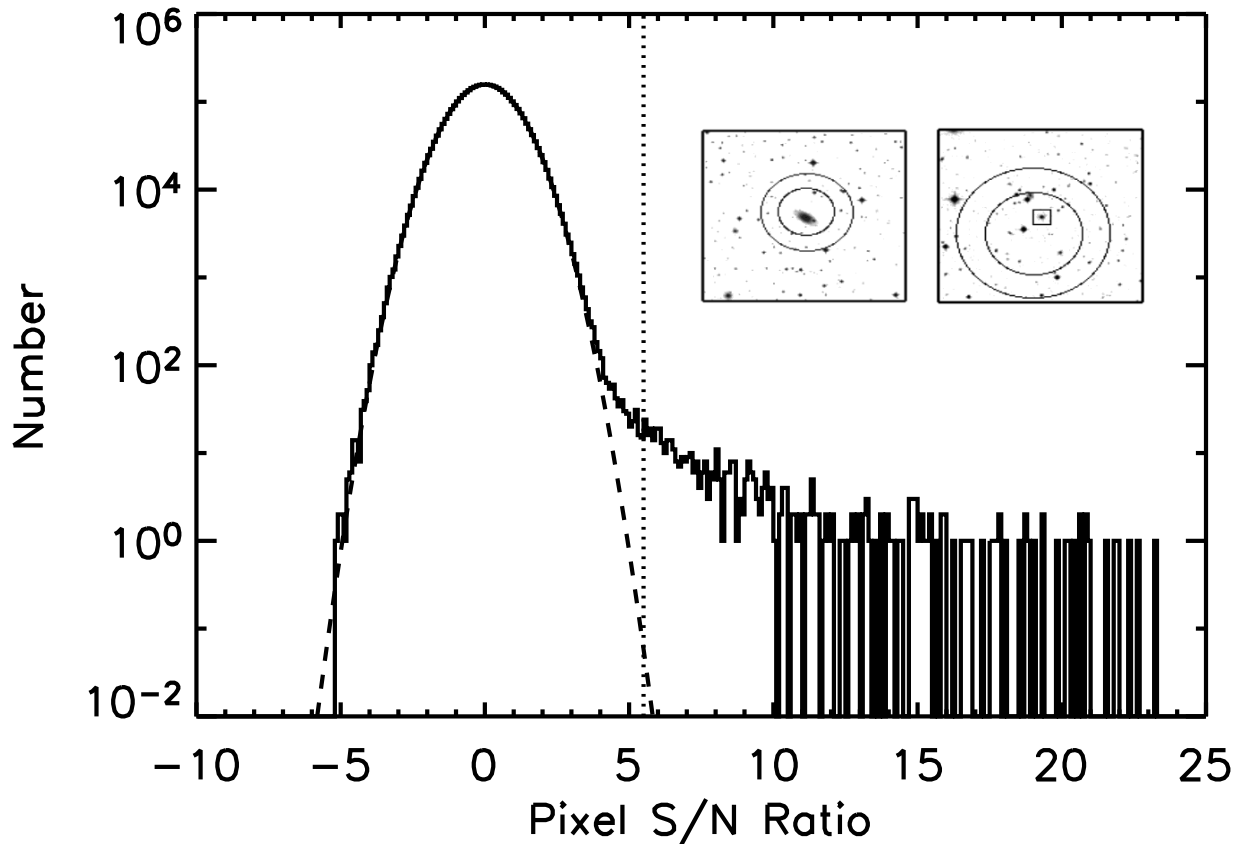


Fig. 2.— Distribution of BAT all-sky map pixel significances. The best-fit gaussian curve (dashed) has a mean and standard deviation of 0.002 and 1.009, respectively. The vertical dotted line is the pixel detection threshold of 5.5σ . Insets: example BAT-detected sources overlaid on DSS images centered on MCG -5-23-016 (left) and 3C 390.3 (right), respectively. The images are $8'$ on a side (east is left, north is up). The larger circles represent the BAT 90% and 99% confidence regions for significances of 26σ (MCG -5-23-016) and 10σ (3C 390.3). The small box identifies 3C 390.3.

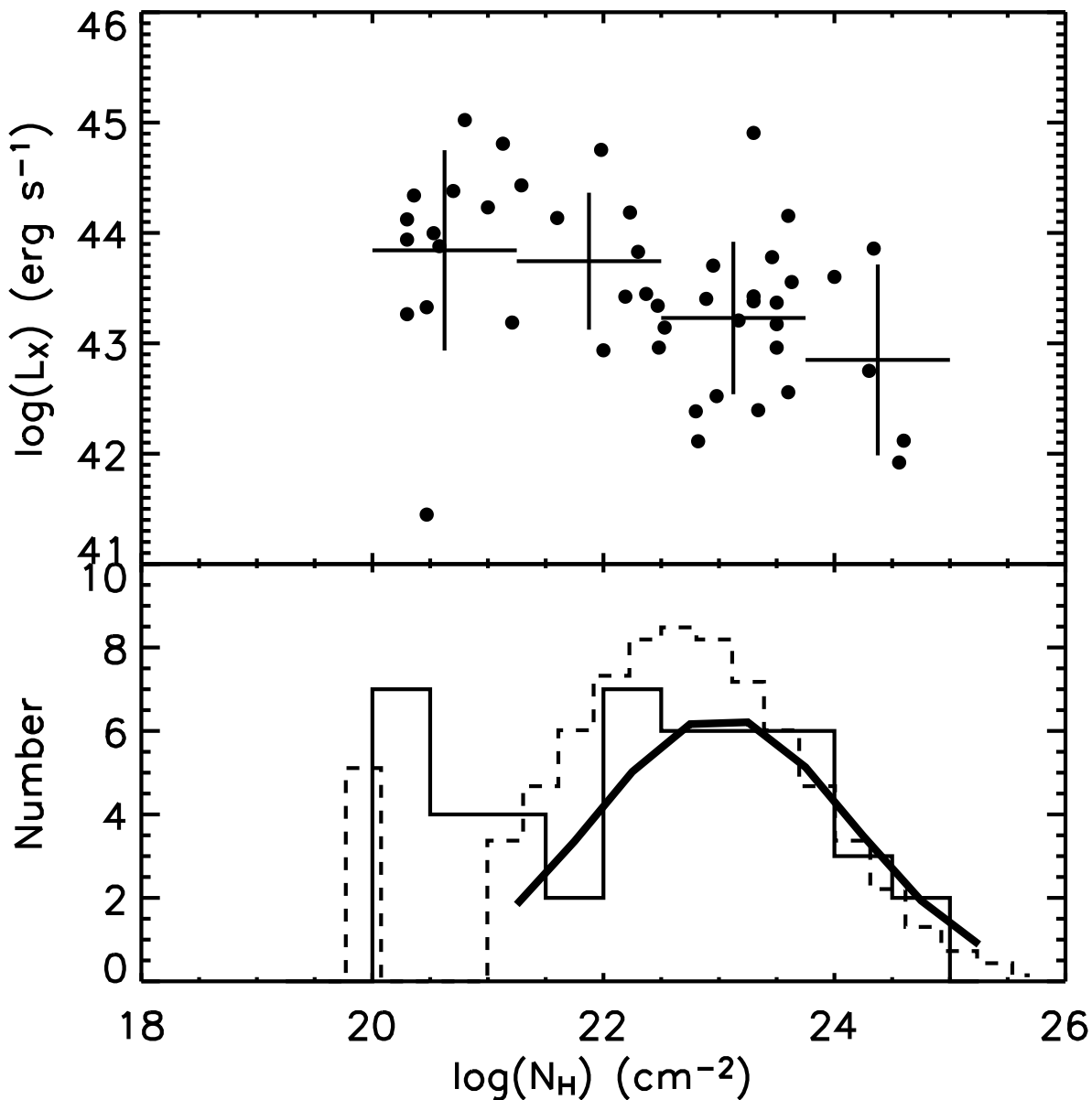


Fig. 3.— Correlation between absorption and BAT hard X-ray luminosity (dots; top). The crosses show mean and standard deviation of the luminosity in several N_H bins. The distribution of absorptions for BAT detected sources is shown in the bottom panel (solid line). Also shown are the distribution predicted by Hopkins et al. (2005a) (dashed), and a gaussian fit to the bins for $\log N_H > 21$ (solid; centroid = 23.0; $\sigma = 1.1$). The peaks at $\log N_H \sim 20 - 21$ are artificial: for the BAT sources, the peak is an upper limit to the measurable absorption in the 2–10 keV band; and for Hopkins, who collect all sources for $\log N_H < 21$ into a single bin.